Design and room-temperature operation of GaAs/AlGaAs multi-quantum well nanowire lasers

Dhruv Saxena*, Nian Jiang, Xiaoming Yuan, Sudha Mokkapati*, Yanan Guo†, Hark Hoe Tan,

Chennupati Jagadish

Department of Electronic Materials Engineering, Research School of Physics and Engineering,

The Australian National University, Canberra, A.C.T. 2601, Australia.

ABSTRACT: We present the design and room-temperature lasing characteristics of single nanowires containing coaxial GaAs/AlGaAs multi-quantum well (MQW) active regions. The TE01 mode, which has a doughnut shaped intensity profile and is polarized predominantly in-plane to the MQWs, is predicted to lase in these nanowire heterostructures and is thus chosen for the cavity design. Through gain/loss calculations, we determine the nanowire dimensions required to minimize loss for the TE01 mode and determine the optimal thickness and number of QWs for minimizing the threshold sheet carrier density. In particular, we show that there is a limit to the minimum and maximum number of QWs that are required for room-temperature lasing. Based on our design, we grew nanowires of a suitable diameter containing eight uniform coaxial

GaAs/AlGaAs MQWs. Lasing was observed at room temperature from optically pumped single nanowires and was verified to be from TE01 mode by polarization measurements. The GaAs MQW nanowire lasers have a factor of 2 lower threshold fluence than previously demonstrated room-temperature GaAs nanowire lasers.

MAIN TEXT: Mainstream semiconductor lasers use quantum confined active regions to obtain superior device performance in terms of threshold, differential gain, modulation bandwidth and temperature stability.[1] These improvements result from the modification of the density of states in structures with reduced dimensionality. In recent years, semiconductor nanowires have emerged as promising structures for reducing the footprint of conventional lasers and for integrating lasers onto Si. Nanowires composed of direct bandgap semiconductors provide both a gain medium and a cavity for lasing and can be grown on Si substrates, despite differences in crystal lattice constants. Systematic improvements in growth of nanowires and cavity optimization have resulted in a myriad of semiconductor nanowire lasers composed of various bulk semiconductor gain mediums.[2-13] In contrast, only a few semiconductor nanowire lasers with quantum confined active regions have been reported.[14-17] While the incorporation of a quantum confined active region is promising for improving the laser performance, the performance of the reported nanowire lasers thus far has not surpassed that of nanowire lasers with bulk active regions. Possible explanations for this could be that the laser cavity was not properly designed for the complex heterostructure, or the placement of the quantum confined active regions in the cavity was not optimal. Mode confinement and mode reflectivity at nanowire end facets is dependent on the refractive index profile of the cavity, and will be different in a nanowire with complex heterostructure compared

to a nanowire with homogenous bulk gain medium. Furthermore, an active region with anisotropic gain will result in very different modal gain characteristics compared to an active region with isotropic gain. For the former, the modal gain will depend on both the polarization and spatial overlap of a mode with the active region.[18] Thus, depending on the type of heterostructure (radial or axial), different modes will be expected to lase compared to nanowire lasers with bulk gain mediums and subsequently the cavity will need to be designed accordingly.

In this article, we present the design of Fabry-Perot type nanowire cavities with radial GaAs/AlGaAs multi-quantum well (MQW) active regions. Our modelling uncovers important design criteria for achieving population inversion in the quantum confined gain regions. We show that for a given structure there is an optimal number of QWs to reduce the threshold pump fluence and an optimal QW thickness to minimize the threshold carrier density. We also show that the lasing mode is determined by the placement of the QWs in the nanowire, unlike bulk nanowire lasers, where the lasing mode is determined solely by the nanowire diameter. Furthermore, we experimentally validate our modelling and demonstrate the lowest-threshold room-temperature GaAs/AlGaAs QW nanowire lasers to date, which have much lower threshold fluence than their bulk counterparts.

Firstly we study the cavity design for a nanowire laser with radial GaAs/AlGaAs MQWs. The heterostructure consists of a GaAs/AlGaAs core-shell, epitaxial GaAs/AlGaAs MQW shells, which serve as the gain medium, and a thin GaAs cap, which prevents oxidation of the Al containing barriers. For the modelling, we have assumed that the nanowire has a hexagonal cross-section, the GaAs MQWs are of uniform thickness and that the AlGaAs barriers have uniform Al concentration of 42%. The nanowire laser is modelled in a horizontal configuration, lying on low index SiO_2 substrate with both nanowire end facets exposed to air. In this configuration the

nanowire behaves as a Fabry-Perot (FP) cavity for the guided modes supported along the nanowire axis. The threshold for laser oscillation occurs when the modal gain balances the modal loss in the cavity. We have used a two-step approach to design the GaAs MQW nanowire lasers. First we model loss for the various guided modes supported in the nanowire. This enables us to identify the mode with lowest loss and select the nanowire dimensions to minimize loss. Then for a nanowire of fixed dimensions, we maximize the modal gain for the mode with lowest loss. The thickness, number and placement of the MQWs in the nanowire are varied and the optimal parameters that reduce threshold carrier density are thereby determined.

The round-trip loss for a mode in a FP type cavity is given by $\alpha_i + \alpha_m$, where α_i is the intrinsic loss and $\alpha_m = L^{-1}\ln(1/R)$ is the mirror loss, where L is the cavity length and R is the geometric mean of mirror reflectances. In homogenous nanowire structures, where the entire nanowire serves as the gain medium, $\alpha_m \gg \alpha_i$ and so the round-trip loss is well estimated by α_m alone.[19] However, in our MQW nanowire heterostructure, α_i can be large due to absorption of the GaAs QW emission in the bulk GaAs core and cap regions. The magnitude of α_i will therefore depend on the dimensions of the core and cap and the mode overlap with these regions. To estimate the modal loss for a GaAs MQW nanowire, we have modelled the loss in GaAs/AlGaAs/GaAs core-shell-cap nanowire, with an 80 nm-diameter core and 5 nm-thick cap. The mode profiles in this simplified 3-layer structure are similar to the mode profiles in the MQW heterostructure, since the thickness of the QWs is much smaller compared to the barriers. For the modelling, the dimensions of the core and cap were fixed while the AlGaAs shell thickness was varied to calculate loss as a function of the overall nanowire diameter (D). Figure 1a shows the modal loss as a function of the nanowire diameter, with $L = 5$ μm, which is the typical length of our nanowires. The mode wavelength was 800 nm for these calculations, which corresponds to the emission wavelength of

4

4 nm-thick GaAs QW.[20] We have also calculated loss at other wavelengths corresponding to 2 and 6 nm-thick GaAs QWs (see Supporting Information), however the estimates are quite similar for the low loss modes, which have a poor overlap with core and cap.

As shown in Figure 1a, the TE01 mode has the lowest loss for all diameters above its cut-off diameter of 240 nm. This is quite different to the modal loss in a nanowire with homogenous bulk gain medium[21] or a core-shell-cap nanowire with the core as the active region[11], where modes other than TE01 mode can have the lowest loss, especially in large diameter nanowires. The difference between the current design and these other nanowire laser designs is due to the absorbing passive regions in our cavity (core and cap). The TE01 mode has the lowest intrinsic loss in our design, because its doughnut-shaped intensity profile has a very poor overlap with the core and cap. The intrinsic loss for all other modes is comparatively larger and consequently the net loss is also larger. The difference in loss between the TE01 mode and other modes is even greater in nanowires with a thicker cap (see Supporting Information), which is favorable for reducing mode competition and obtaining single transverse-mode operation.[22] Thus our cavity design is best suited for obtaining lasing from the TE01 mode. For the current design, the nanowire diameter should be larger than 400 nm to minimize loss for the TE01 mode.

The TE01 mode, because of its intensity profile and polarization, is also the most suitable mode for obtaining large modal gain from the GaAs MQWs embedded in the shell of the nanowire. The inset of Figure 1b shows the electric field profile (magnitude and direction) of the TE01 mode in the cross-section of the nanowire containing a single coaxial QW. The nanowire has an 80 nm diameter core, 5 nm thick cap and an overall diameter of 420 nm. The maximum intensity of the TE01 mode is approximately a distance $D/4$ from the centre of the nanowire and coincides with the position of the coaxial QW. Moreover, the electric field is azimuthally polarized and is

approximately parallel to the coaxial QW. The material gain (g) in QWs is polarisation dependent and is larger for electric field polarised parallel to the QW plane than perpendicular to the QW plane in GaAs QWs ($g_\parallel > g_\perp$).[1] Thus, modal gain for the TE01 mode is expected to be large in our design. To verify this, we calculated the modal gain for all guided modes supported in the nanowire. We defined separate confinement factors, $\Gamma_\parallel$ and $\Gamma_\perp$, for polarization in-plane and out-of-plane to the QWs, and calculated modal gain using $\Gamma_\parallel g_\parallel + \Gamma_\perp g_\perp$ (see Supporting Information). Our calculations show that the TE01 mode has the largest modal gain in our cavity design, provided that the QWs are suitably placed in the nanowire.

To maximize the modal gain for the TE01 mode, the QWs need to be ideally placed at the maxima of the mode intensity profile. However, due to the much smaller volume of the QW in comparison to the mode, a single QW placed at the optimal position has a very small confinement factor ($\Gamma \sim 0.05$; $\Gamma = \Gamma_\parallel$ for TE01 mode). To increase the modal gain, multiple QWs can be used, provided that the barriers are sufficiently thick to avoid coupling.[23] We have calculated the mode confinement factor with 3, 5 and 8 uniformly spaced MQWs in the nanowire (see Supporting Information Table 1). Γ can be increased to 0.3 using 8 MQWs, albeit the increase is not linear with the number of QWs (n_w) because the electric field intensity of the TE01 mode is not constant across the active region. While increasing n_w increases Γ, there is a practical limit to how large n_w (and thus Γ) can be due to the finite diameter of the nanowire and the mode intensity profile. More importantly, for a given nanowire diameter and length (or given threshold modal gain requirement), there is an optimum n_w for minimising the threshold pump fluence (or current density for electrical injection)[24, 25]. For a 420 nm diameter nanowire, we estimate that 8 is the maximum number of uncoupled coaxial QWs that can be accommodated and also the optimum n_w for minimising the threshold pump fluence at room temperature (see Supporting Information).

Figure 1b shows the TE01 modal gain in a 420 nm diameter nanowire with 2, 4 or 6 nm thick GaAs QWs and n_w = 1, 3, 5 or 8 as a function of sheet carrier density. The loss for the TE01 mode in a 420 nm diameter, 5 μm long nanowire at mode wavelengths of 730, 800 and 830 nm, corresponding to QWs of thickness 2, 4 and 6 nm respectively, is represented by the grey lines. The loss is larger at shorter mode wavelengths as a result of larger absorption coefficient in GaAs core and cap. The intersection of the gain and loss curves defines the threshold sheet carrier density. Clearly, the threshold cannot be attained with a single QW. At least 3 MQWs are required to achieve lasing for 6 nm-wide QWs and 5 MQWs are required for 2 nm- and 4 nm-wide QWs. The larger gain for 6 nm-wide QWs at sheet carrier densities above 2.5×10^{13} cm^{-2} is due to higher subband transitions, which are not supported in thinner QWs (at room temperature). The threshold sheet carrier density can be reduced using 8 MQWs, which is the maximum number of uncoupled QWs that can be accommodated in this diameter nanowire. The lowest sheet carrier density of 8.2×10^{12} cm^{-2} is achieved with 4 nm-wide 8 MQWs. The threshold sheet carrier density is larger for 2 nm-wide 8 MQWs because of the larger modal loss and for 6 nm-wide 8 MQWs because of the lower material gain. Thus, 4 nm is the optimal width and 8 is the optimal number of MQWs for our nanowire laser design.

We aimed to grow GaAs MQW nanowires according to the optimized design. GaAs/AlGaAs core-shell nanowires with eight coaxial GaAs/AlGaAs QWs and a thin GaAs cap were grown in a metal organic chemical vapor deposition (MOCVD) system (see methods). Since the shell growth rate has a non-linear dependence with nanowire diameter, the growth time for each QW/barrier layer had to be carefully varied, in order to obtain uniformly separated MQWs of uniform thickness. The nanowires were imaged after growth in a scanning electron microscope (SEM). Figure 2a shows the 45° tilt view SEM image of a nanowire standing on the growth substrate. The nanowire

has a 1 µm-thick broad tapered base, a 1.5 µm-long short tapered segment, and a 3.3 µm-long untapered segment. The top end of the nanowire has multiple smooth inclined crystallographic facets, terminating at the 80 nm Au nanoparticle. All the nanowires grown had similar morphological characteristics, except the shape of the top end varied across the sample. The nanowires provided suitable laser cavities once transferred onto glass substrates for optical characterization. The SEM images of transferred nanowires (see Supporting Information) shows that all nanowires break away from above the tapered base. In some nanowires the top end of the nanowire is also broken off, leaving behind an untapered segment, which serves as an ideal nanowire cavity. The transferred nanowires had an average diameter of 500 nm and average length of 4.7 µm. These dimensions are suitable for obtaining low loss (or low threshold modal gain) for the TE01 mode according to our design.

To reveal the details of the MQW heterostructure, we performed transmission electron microscopy (TEM) studies on cross-sectional samples prepared using ultramicrotomy (see methods). Figure 2b shows the high-angle annular dark field scanning transmission electron microscopy (HAADF-STEM) image of a typical cross-sectional sample, with a schematic illustration of the cross-section superimposed on the right side. In this Z-contrast image, where Z is the atomic number, the brighter regions correspond to GaAs and the darker regions correspond to $Al_xGa_{1-x}As$ (x>0). The GaAs/AlGaAs layers in the core-shell heterostructure are identified in the schematic. The GaAs core has a hexagonal shape and is encapsulated by a thick AlGaAs shell, 8x GaAs/AlGaAs MQWs and a thin GaAs cap. The diameter of the GaAs core is 80 nm, the first AlGaAs shell is 44 nm thick and the GaAs cap is ~3 nm thick, as measured along the <110> direction from the STEM image. The first AlGaAs shell is thick enough to prevent carriers tunneling from the MQWs into the GaAs core. We performed EDX analysis to quantify the Al concentration in the $Al_xGa_{1-x}As$

shells. The regions near the Al-rich radial bands were not sampled to avoid skewing the estimate. By benchmarking against the As concentration measured in the GaAs core, we measured an average Al concentration of 0.42 ± 0.01 in the AlGaAs shells.

Figure 2c shows the HAADF-STEM image of the cross-section sample at higher magnification, in which the eight GaAs MQWs and the thin GaAs cap are clearly resolved. The thickness of individual QWs and barriers is non-uniform, due to differing growth rates across different crystallographic directions.[26] To quantify the QW/barrier thickness, we measured thickness at several different positions on the STEM images using line scans along <110> direction (see Supporting Information). The average thickness of the MQWs is 3.5 ± 1.5 nm. The average thickness of the AlGaAs barriers ranges from 9-20 nm. In particular, the first four MQWs are separated by thicker barriers (average thickness 14 nm) than the last four MQWs (average thickness 9 nm). The placement of the inner six MQWs overlaps well with the field profile of the TE01 mode in this diameter nanowire (see Supporting Information). Several nanowire cross-sections were analyzed and all of them had similar structural characteristics. From statistical analysis of our measurements, we find that the mean and standard deviation of thicknesses for each coaxial QW is approximately the same. Homogeneity between MQWs is necessary for realizing large modal gain and reducing the threshold power required to achieve lasing. Based on the placement of the MQWs in the nanowire and reasonable homogeneity between MQWs, we expect these GaAs MQW nanowires to lase at room temperature.

Nanowires were transferred onto ITO coated glass substrates and individual nanowires were optically pumped at room temperature in a micro-photoluminescence (μ-PL) system (see methods). The emission spectrum from a single nanowire at three different pump fluences is presented in Figure 3a and the normalized spectral map is presented in the top left inset. At very

low pump fluence (<5 µJ/cm^2/pulse), the spectrum has a broad single peak (FWHM = 50 nm) centered at 800 nm, corresponding to the ground state emission from the MQWs. The broad linewidth is mainly due to variation in the QW thicknesses across the nanowire facets (see Supporting Information). At a pump fluence of ~20 µJ/cm^2/pulse, several low-amplitude peaks appear in the broad PL spectrum. These peaks become more pronounced with increasing pump fluence, and thus correspond to amplified cavity modes in the nanowire. At a pump fluence of ~110 µJ/cm^2/pulse, the peaks at 791 nm and 819 nm rapidly increases in intensity, above the background emission level. The linewidth of these lasing peaks measured at pump fluence of 154 µJ/cm^2/pulse is 1 nm. At higher pump fluence, several narrow lasing peaks appear in the spectra and the intensity of the dominant lasing peaks is orders of magnitude larger than the background spontaneous emission. The multiple peaks in the lasing spectra correspond to different axial and transverse modes in the cavity. The optical image of the nanowire above threshold (bottom inset in Figure 3a) shows intense emission from the nanowire ends and a distinct interference pattern, which confirms that the nanowire behaves as a FP cavity and that lasing is from guided modes supported along the nanowire axis.[27] The peaks at 777, 791, 805 and 819 nm are regularly spaced and correspond to the same transverse mode with different axial order.[28] A group index (n_g) of 4.7 is calculated from the separation of these peaks, which is identical to the n_g calculated for the TE01 mode in this diameter nanowire (see Supporting Information). The subsidiary peaks at shorter wavelengths have a larger n_g and may correspond to the higher order HE modes that could potentially lase in this diameter nanowire.

To verify the lasing modes in the nanowire we analyzed the polarization of emission, by placing a linear polarizer before the entrance slit of the spectrometer (see methods). The integrated spectral emission from the dominant lasing peaks at a pump fluence of 205 µJ/cm^2/pulse is shown as

function of polarization in the top right inset of Figure 3a. The nanowire is orientated horizontally in the polar plot. The emission is polarized perpendicular to the nanowire and has a polarization ratio, $\rho = (I_{\parallel} - I_{\perp})/(I_{\parallel} + I_{\perp})$, of -0.4. The polarisation dependence above threshold is quite different to the polarisation dependence below threshold, which is also shown on the polar plot. The emission below threshold has a very low $|\rho|$, which could be due to multiple factors. Firstly, the nanowire characterised has a large diameter and large diameter nanowires exhibit lower polarisation anisotropy.[29] Secondly, the emission from the radial GaAs MQWs could be coupled to several different modes in the large diameter nanowire and the net emission may not have a dominant linear polarization. The distinct change in the polarization of emission from below threshold to above threshold indicates the strong amplification of a particular transverse mode in the cavity. To identify the lasing mode, we simulated the far-field emission profile of all the various guided modes supported in the nanowire and analyzed their polarization dependence (see Supporting Information). Of all the modes simulated, the polarization dependence of the TE01 mode matched best with the experimental data, and is shown in the polar plot. The slight differences between the experimental and simulated data could be due to the imperfect end facets of the nanowire laser (see Supporting Information) which were not modelled in the simulation. Thus, the TE01 mode is confirmed to be the dominant lasing mode in our MQW nanowire laser, as designed.

The integrated spectral emission from the nanowire as a function of pump fluence (L-L curve) is shown in Figure 3b. The 'S' shaped non-linear response of the laser on the log-log scale and the 'knee' like behavior on the linear scale (inset of Figure 3b) are clearly observed. The region highlighted in grey is the threshold region. The threshold fluence is estimated to be ~110 µJ/cm^2/pulse, which is lower than the threshold fluence of previously demonstrated room-

temperature bulk III-V semiconductor nanowire lasers that were characterized in the same μ-PL system.[11, 12, 30] By comparing the device parameters, we find that the reduction in threshold fluence is mainly due to reduction in the active region volume (see Supporting Information). To assess the performance of the MQW nanowire laser, we used multimode rate-equations to fit the experimental L-L data (see Supporting Information). The analytical fit to the data is shown in Figure 3b. A very good fit was obtained with a threshold gain (g_{th}) of 5200 cm^{-1} and a spontaneous emission factor (β) of 0.03. The average carrier density in the active region at threshold is estimated to be 3.5×10^{19} cm^{-3}, which corresponds to a threshold sheet carrier density of 17.5×10^{12} cm^{-2} assuming a QW thickness of 5 nm. While β is similar to other nanowire lasers of similar dimensions, g_{th} is larger in comparison to bulk nanowire lasers as result of the much lower Γ. Assuming Γ of 0.25 for the TE01 mode in our nanowire, the threshold modal gain (Γg_{th}), or net loss, is estimated to be 1300 cm^{-1}. The loss is slightly larger than the estimated loss of 1000 cm^{-1} in this diameter nanowire, mainly as a result of its imperfect end facets. We note that above threshold, the slope of the L-L curve deviates from a linear regime at high pump fluence. This is due to Auger recombination, which becomes significant at carrier densities larger than 2.5×10^{19} cm^{-3} in GaAs[31]. To improve the performance of the MQW laser, the threshold carrier density must be reduced further, which could be obtained by making the end facets flatter post-growth. Additionally, the nanowire shell growth could be further improved to maximize the overlap of the MQWs with the TE01 mode and minimize the structural variation between MQWs, in order to obtain larger modal gain. Despite the potential for further improvements, the MQW nanowire lasers have lower threshold fluence/carrier density than previously reported III-V semiconductor nanowire lasers with quantum confined active regions[16, 17] (see Supporting Information).

In summary, we have presented the design of a GaAs/AlGaAs MQW nanowire laser and demonstrated low-threshold room-temperature lasing from nanowires containing 8 GaAs/AlGaAs coaxial MQWs. The TE01 mode, due to its intensity profile and polarization, is shown to be the ideal mode for obtaining the lowest threshold gain in these nanowire heterostructures. We have therefore optimized the design of the MQW nanowire lasers to obtain low-threshold lasing from TE01 mode, and verified lasing from this mode in our experiments. Our demonstration paves way for the development of high performance nanowire lasers with tunable emission wavelengths, which are required for future nanophotonic integrated circuits. While we have focused on GaAs/AlGaAs material system here, our systematic approach to the design can be adapted to realize high performance room-temperature MQW nanowire lasers in other material systems, and/or in other cavity configurations, such as vertically orientated nanowires on Si/SiO_2 substrates.

Methods

Nanowire growth. GaAs/AlGaAs MQW nanowire heterostructures were grown in a horizontal flow low pressure (100 mbar) metal organic chemical vapor deposition (MOCVD) system (Aixtron 200/4). Trimethylgallium, trimethylaluminium, and arsine were used as the source of Ga, Al, and As, respectively. Firstly, untapered vertical GaAs nanowires were grown on a (111)B GaAs substrates using 80 nm Au nanoparticle catalysts via a two-temperature growth process[32]. An epitaxial AlGaAs shell followed by 8x GaAs/AlGaAs QW/barrier layers and a thin GaAs cap were then grown in situ around the GaAs (core) nanowires at high temperature (750 °C). The total group III molar fraction used for the GaAs core growth was 1.73×10^{-5} and for the GaAs/AlGaAs multi-shell growth was 1.1×10^{-5} and 2.2×10^{-5}, respectively. The Al concentration was 50% of the total group III in vapor. The group V molar fraction used for the core and shell growth was $8\times10^{-}$

[4] and 2.27×10^{-3}, respectively. The growth time for the multi-shell growth is provided in Supporting Information Table 2.

Electron microscopy and microtomy. Nanowires were first embedded in resin and baked at 70 °C for over 24 hours to allow complete solidification of the resin. The substrate was then removed by dipping the epoxy block into liquid nitrogen for a few seconds. The face of the epoxy block with the embedded nanowires was trimmed to a small isosceles trapezium and then cut into 30 nm thick slides using ultramicrotome (Leica EM UC7) and a diamond knife (DiATOME ultra 45°). The slices from the bottom 1.5 μm were abandoned since the base of the nanowires is tapered and only slices from the untapered segment (2-2.5 μm) were transferred onto copper grids for TEM analysis. The cross-sectional samples were characterized at an acceleration voltage of 200 kV using JEOL 2100F equipped with an energy-dispersive X-ray (EDX) detector.

Optical characterization. Nanowires were dispersed in IPA solution using ultrasonication and then transferred via solution onto an indium tin oxide (ITO) coated glass substrate. Individual nanowires were pumped using a frequency-doubled solid-state laser (femtoTRAIN IC-Yb-2000, λ = 522 nm, repetition rate 20.8 MHz, pulse length 400 fs) through a 100x/0.90 numerical aperture objective lens (Nikon LU Plan). In order to pump the nanowires uniformly, the excitation beam spot-size was enlarged to 5 μm by placing a spherical lens (f = 500 mm) in the incoming beam pathway. The emission from the nanowire was collected through the same objective lens and was spectrally filtered to remove the pump laser wavelength. Spectral measurements were made using a grating spectrometer (Acton, SpectraPro 2750) equipped with 150 lines/mm grating and a charged coupled device (Princeton Instruments, PIXIS). For polarization analysis, the sample was mounted on a rotating stage and the nanowire was orientated 45° with respect to the plane of polarization of the pump laser. A linear polarizer was inserted in the collection path in the optical

system, and the polarization axis of the polarizer was rotated to match the orientation of the nanowire.
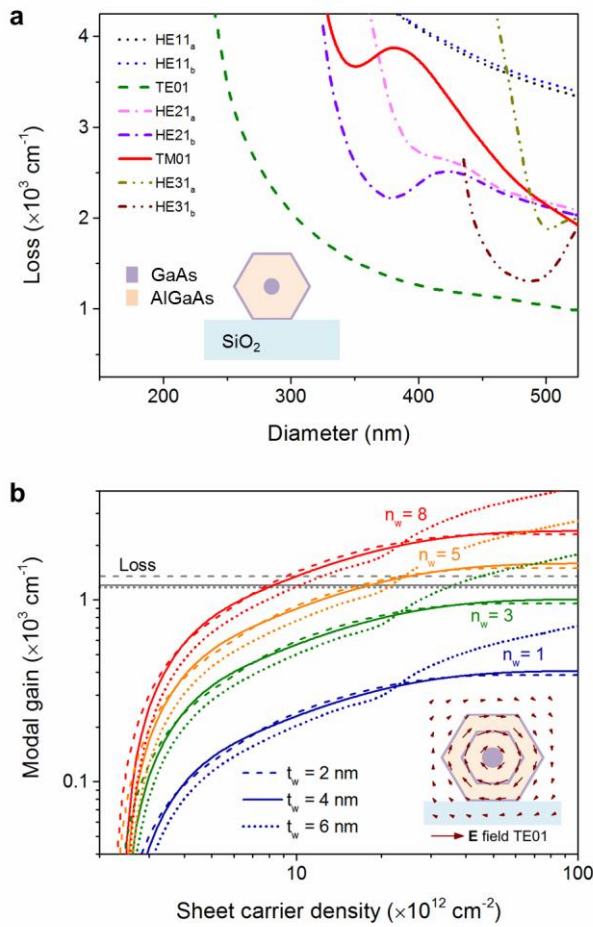
Figure 1. Design for GaAs multi-QW nanowire laser. a. Modal loss in a core-shell-cap GaAs/AlGaAs/GaAs nanowire with 80 nm diameter core and 5 nm-thick cap. The AlGaAs shell thickness is varied to calculate loss as a function of the nanowire diameter. The nanowire has a hexagonal cross-section and is lying on a SiO$_2$ substrate, as shown in the inset. The mirror loss is calculated using $\alpha_m = L^{-1}\ln(1/R)$, where R is the mode reflectance at the nanowire/air end facet and L is the nanowire length. R was calculated using FDTD simulations (see Supporting Information) and $L = 5$ μm was used for these calculations. The intrinsic loss as a result of absorption in GaAs core and cap was calculated using Mode Solutions at mode wavelength of 800 nm. **b**. Modal gain for TE01 mode as a function of sheet carrier density for different number of

QWs (n_w = 1, 3, 5 and 8) and for QW thickness of 2, 4 and 6 nm. The material gain is calculated at 300 K. The mode confinement factor is calculated at wavelength of 730, 800 and 830 nm for QWs of 2, 4 and 6 nm thickness, respectively. The horizontal lines in grey are the modal loss for TE01 mode in 420 nm diameter nanowire at wavelengths corresponding to 2, 4 and 6 nm thick QWs. The inset shows the electric field profile (magnitude and direction) of the TE01 mode in the cross-section of a nanowire with a single coaxial QW, with the QW placed equidistant from the core and cap.
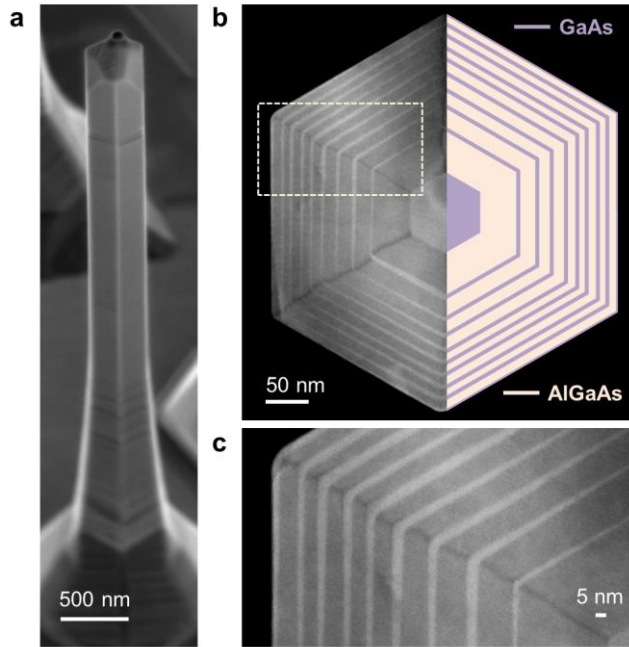
Figure 2. Structural characterization of GaAs multi-QW nanowires. a. Scanning electron microscope image at 45° tilt angle of a nanowire standing on the growth substrate. The nanowire has a 1 μm-thick broad base, a slightly tapered segment 1.5 μm long and an untapered segment 3.3 μm long. All the nanowires grown had similar morphological characteristics (see Supporting Information). **b**. HAADF-STEM image of a 30 nm-thick cross-section taken from the untapered segment of a nanowire. A schematic illustration of the cross-section has been superimposed on the right half of the STEM image. The heterostructure contains an 80 nm-GaAs core, an AlGaAs shell, 8x GaAs/AlGaAs co-axial MQWs and a thin GaAs cap. **c**. HAADF-STEM image of the cross-section in **b** at higher magnification, showing the MQWs of approximate thickness 5 nm and the 3 nm-thick GaAs cap.
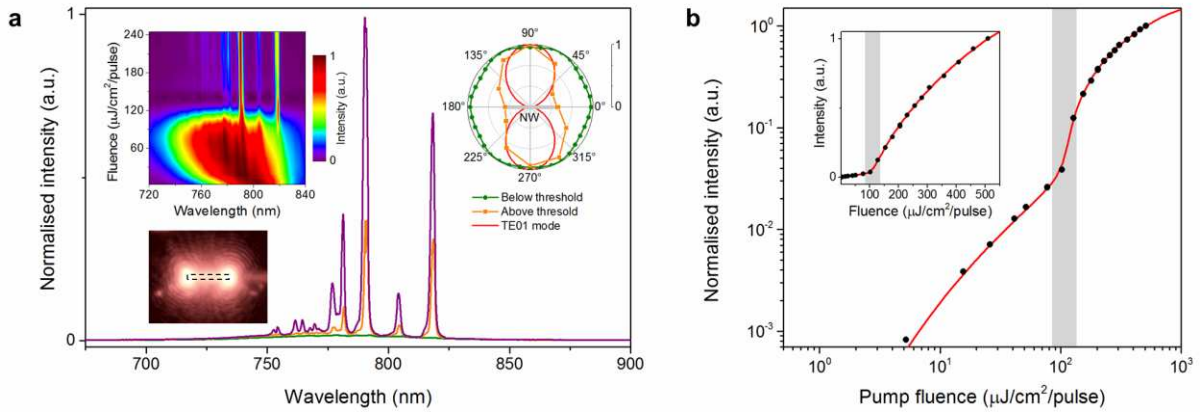
Figure 3. Room-temperature lasing characteristics. a. Spectra at three different pump intensities, corresponding to below threshold (green: 77 µJ/cm²/pulse), just above threshold (orange: 128 µJ/cm²/pulse) and far above threshold (purple: 180 µJ/cm²/pulse). The top left inset shows the normalized spectral map as a function of the optical pump fluence. A sudden narrowing of spectral emission is observed at threshold fluence of 110 µJ/cm²/pulse. The bottom left inset shows the optical microscope image of the nanowire laser above threshold (with the pump laser filtered out). The outline of the nanowire is indicated by the dashed lines. The top right inset shows the total emission intensity from the nanowire, below and above threshold, as a function of polarization angle. The nanowire is orientated horizontally in the image, so that angle of 0 or 180° corresponds to polarization parallel to the axis of the nanowire. The polarization dependence of the TE01 mode is also shown for comparison. **b.** Non-linear response of laser output intensity versus pump fluence on log-log scale, and on a linear scale (inset). The 'S' like curve characteristic of lasing is clearly observed. The grey region highlights the region of amplified spontaneous emission. The dots represent the experimental data and the line is fit to the experimental data using multi-mode rate-equations with g_{th} = 5200 cm⁻¹ and β = 0.03 (see Supporting Information).

ASSOCIATED CONTENT

Supporting Information. Additional information on the design of GaAs MQW nanowire lasers, loss/modal gain calculations for other guided modes, axial and transverse mode confinement factors, optimum placement and number of MQWs, structural characterization of nanowires, measurements of QW and barrier thicknesses, measurement of nanowire laser dimensions, characterization of lasing mode based on group index calculations, polarization dependence of various photonic modes, rate equation analysis and comparison between bulk and MQW GaAs nanowire lasers. This material is available free of charge via the Internet at http://pubs.acs.org.

AUTHOR INFORMATION

Corresponding Author

*dhruv.saxena@anu.edu.au ; *sudha.mokkapati@anu.edu.au

Present Addresses

[†]Samsung Austin Semiconductor LLC, 12100 Samsung Blvd #110, Austin, TX 78754, United States of America.

Author Contributions

D.S., S.M., H.T. and C.J. conceived and designed the experiments. D.S. did the modelling. N.J. grew the nanowires. X.Y. and Y.G. prepared cross-sectional samples and conducted the TEM analysis. D.S. performed the experiments and analyzed the results in consultation with S.M.. H.T. and C.J. supervised the work. D.S wrote the manuscript with contributions from all authors.

work, and Centre for Advanced Microscopy (CAM) and Australian National Fabrication Facility (ANFF) for providing access to the growth and fabrication facilities.

ABBREVIATIONS

MQW, multi-quantum well, FP, Fabry-Perot; MOCVD, metal organic chemical vapor deposition; SEM, scanning electron microscope; HAADF-STEM, high-angle annular dark field scanning transmission electron microscopy, PL, photoluminescence.

REFERENCES

1.	Coldren, L. A.; Corzine, S. W.; Masanovic, M. L., *Diode lasers and photonic integrated circuits*. Second ed.; Wiley: New Jersey, 2012.

2.	Johnson, J. C.; Choi, H.-J.; Knutsen, K. P.; Schaller, R. D.; Yang, P.; Saykally, R. J. *Nat Mater* **2002,** 1, (2), 106-110.

3.	Duan, X.; Huang, Y.; Agarwal, R.; Lieber, C. M. *Nature* **2003,** 421, (6920), 241-245.

4.	Gradecak, S.; Qian, F.; Li, Y.; Park, H.-G.; Lieber, C. M. *Applied Physics Letters* **2005,** 87, (17), 173111.

5.	Chin, A. H.; Vaddiraju, S.; Maslov, A. V.; Ning, C. Z.; Sunkara, M. K.; Meyyappan, M. *Applied Physics Letters* **2006,** 88, (16), 163115-3.

6.	Zimmler, M. A.; Bao, J.; Capasso, F.; Muller, S.; Ronning, C. *Applied Physics Letters* **2008,** 93, (5), 051101-3.

7.	Chen, R.; Tran, T.-T. D.; Ng, K. W.; Ko, W. S.; Chuang, L. C.; Sedgwick, F. G.; Chang-Hasnain, C. *Nat Photon* **2011,** 5, (3), 170-175.

8.   Xiao, Y.; Meng, C.; Wang, P.; Ye, Y.; Yu, H.; Wang, S.; Gu, F.; Dai, L.; Tong, L. *Nano Letters* **2011,** 11, (3), 1122-1126.

9.   Sebastian, G.; Andreas, T.; Robert, R.; Christian, B.; Amanda, M.; Michael, K.; Julian, K.; Kristen, A. S.; Federico, C.; Carsten, R. *Nanotechnology* **2012,** 23, (36), 365204.

10.   Liu, Z.; Yin, L.; Ning, H.; Yang, Z.; Tong, L.; Ning, C.-Z. *Nano Letters* **2013,** 13, (10), 4945-4950.

11.   Saxena, D.; Mokkapati, S.; Parkinson, P.; Jiang, N.; Gao, Q.; Tan, H. H.; Jagadish, C. *Nat Photon* **2013,** 7, (12), 963-968.

12.   Gao, Q.; Saxena, D.; Wang, F.; Fu, L.; Mokkapati, S.; Guo, Y.; Li, L.; Wong-Leung, J.; Caroff, P.; Tan, H. H.; Jagadish, C. *Nano Letters* **2014,** 14, (9), 5206-5211.

13.   Li, K. H.; LiuX; WangQ; ZhaoS; MiZ. *Nat Nano* **2015,** 10, (2), 140-144.

14.   Choi, H.-J.; Johnson, J. C.; He, R.; Lee, S.-K.; Kim, F.; Pauzauskie, P.; Goldberger, J.; Saykally, R. J.; Yang, P. *The Journal of Physical Chemistry B* **2003,** 107, (34), 8721-8725.

15.   Qian, F.; Li, Y.; Gradecak, S.; Park, H.-G.; Dong, Y.; Ding, Y.; Wang, Z. L.; Lieber, C. M. *Nat Mater* **2008,** 7, (9), 701-706.

16.   Tatebayashi, J.; Kako, S.; Ho, J.; Ota, Y.; Iwamoto, S.; Arakawa, Y. *Nat Photon* **2015,** 9, (8), 501-505.

17.   Stettner, T.; Zimmermann, P.; Loitsch, B.; Döblinger, M.; Regler, A.; Mayer, B.; Winnerl, J.; Matich, S.; Riedl, H.; Kaniber, M.; Abstreiter, G.; Koblmüller, G.; Finley, J. J. *Applied Physics Letters* **2016,** 108, (1), 011108.

18.   Maslov, A. V.; Ning, C. Z. *IEEE J. Quantum Electron.* **2004,** 40, (10), 1389-1397.

19.   Mariano, A. Z.; Federico, C.; Sven, M.; Carsten, R. *Semicond. Sci. Technol.* **2010,** 25, (2), 024001.

20.   Davies, C. L.; Parkinson, P.; Jiang, N.; Boland, J. L.; Conesa-Boj, S.; Tan, H. H.; Jagadish, C.; Herz, L. M.; Johnston, M. B. *Nanoscale* **2015,** 7, (48), 20531-20538.

21.   Saxena, D.; Wang, F.; Gao, Q.; Mokkapati, S.; Tan, H. H.; Jagadish, C. *Nano Letters* **2015,** 15, (8), 5342-5348.

22.   Siegman, A. E., *Lasers*. University Science Books: Mill Valley, California, 1986.

23.   Arakawa, Y.; Yariv, A. *Quantum Electronics, IEEE Journal of* **1986,** 22, (9), 1887-1899.

24.   Arakawa, Y.; Yariv, A. *Quantum Electronics, IEEE Journal of* **1985,** 21, (10), 1666-1674.

25.   Ilroy, P. M.; Kurobe, A.; Uematsu, Y. *Quantum Electronics, IEEE Journal of* **1985,** 21, (12), 1958-1963.

26.   Zheng, C.; Wong-Leung, J.; Gao, Q.; Tan, H. H.; Jagadish, C.; Etheridge, J. *Nano Letters* **2013,** 13, (8), 3742-3748.

27.   van Vugt, L. K.; Rühle, S.; Vanmaekelbergh, D. *Nano Letters* **2006,** 6, (12), 2707-2711.

28.   van Vugt, L. K.; Zhang, B.; Piccione, B.; Spector, A. A.; Agarwal, R. *Nano Letters* **2009,** 9, (4), 1684-1688.

29.   Chen, G.; Wu, J.; Lu, Q.; Gutierrez, H. R.; Xiong, Q.; Pellen, M. E.; Petko, J. S.; Werner, D. H.; Eklund, P. C. *Nano Letters* **2008,** 8, (5), 1341-1346.

30.   Burgess, T.; Saxena, D.; Mokkapati, S.; Li, Z.; Hall, C. R.; Davis, J. A.; Wang, Y.; Smith, L. M.; Fu, L.; Caroff, P.; Tan, H. H.; Jagadish, C. *Nat Commun* **2016,** 7.

31.   Strauss, U.; Ruhle, W. W.; Kohler, K. *Applied Physics Letters* **1993,** 62, (1), 55-57.

32.   Joyce, H. J.; Gao, Q.; Tan, H. H.; Jagadish, C.; Kim, Y.; Zhang, X.; Guo, Y.; Zou, J. *Nano Letters* **2007,** 7, (4), 921-926.
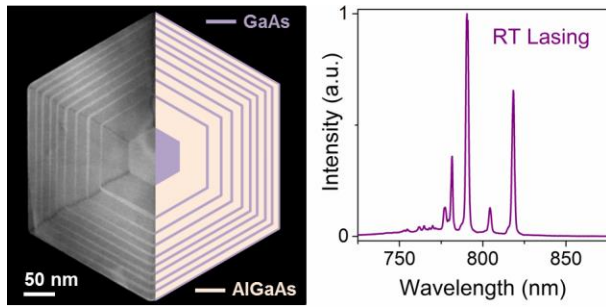
Cross-sectional image of GaAs/AlGaAs multi-quantum well (MQW) nanowire heterostructure (left) and room-temperature lasing spectrum from a GaAs/AlGaAs MQW nanowire (right).